Velocity map photoelectron-photoion coincidence imaging on a single detector

Lehmann, C.S.; Ram, N.B.; Janssen, M.H.M.

published in
Review of Scientific Instruments
2012

DOI (link to publisher)
10.1063/1.4749843

document version
Publisher's PDF, also known as Version of record

AIP | Review of Scientific Instruments

Velocity map photoelectron-photoion coincidence imaging on a single detector

C. Stefan Lehmann, N. Bhargava Ram, and Maurice H. M. Janssen

Citation: Rev. Sci. Instrum. **83**, 093103 (2012); doi: 10.1063/1.4749843
View online: http://dx.doi.org/10.1063/1.4749843
View Table of Contents: http://rsi.aip.org/resource/1/RSINAK/v83/i9
Published by the American Institute of Physics.

Velocity map photoelectron-photoion coincidence imaging on a single detector

C. Stefan Lehmann, N. Bhargava Ram, and Maurice H. M. Janssen[a)]
LaserLaB Amsterdam, VU University Amsterdam, de Boelelaan 1083, 1081 HV Amsterdam, The Netherlands

(Received 2 July 2012; accepted 19 August 2012; published online 5 September 2012)

Here we report on a new simplified setup for velocity map photoelectron-photoion coincidence imaging using only a *single* particle detector. We show that both photoelectrons and photoions can be extracted toward the same micro-channel-plate delay line detector by fast switching of the high voltages on the ion optics. This single detector setup retains essentially all the features of a standard two-detector coincidence imaging setup, viz., the high spatial resolution for electron and ion imaging, while only slightly decreasing the ion time-of-flight mass resolution. The new setup paves the way to a significant cost reduction in building a coincidence imaging setup for experiments aiming to obtain the complete correlated three-dimensional momentum distribution of electrons and ions. [http://dx.doi.org/10.1063/1.4749843]

I. INTRODUCTION

Charged particle imaging spectrometers or "reaction microscopes" employing the velocity map imaging technique have become a proliferating tool in reaction dynamics studies today. The determination of the full three-dimensional momentum distribution of the fragment products (ions and electrons in a ionization event) in coincidence provides complete kinematic information of the event. Time-resolved coincidence measurements are particularly useful in studying the dynamical behavior in many body systems like polyatomic molecules. Many versions of photoelectron-photoion coincidence spectrometers have evolved over the last two decades to study molecular photoexcitation and ionization processes.[1–13] The temporal and spatial resolution of electrons/ions imaged has also improved enormously, especially by incorporating the velocity map imaging technique.[14,15] In 2008, a photoelectron-photoion coincidence imaging apparatus to study femtosecond molecular dynamics was constructed in our laboratory in LaserLaB Amsterdam with temporal resolution down to tens of picoseconds (∼16 ps for electrons) and spatial resolution of ions down to few hundred microns (∼115 μm for Xe^+ ions).[11] Using time switched voltages on open lenses, electrons and ions were velocity focussed onto two micro-channel-plate delay line detectors in opposite directions. A common characteristic of almost all coincidence detection setups reported in literature is the usage of two opposite facing time-of-flight (ToF) detectors. In a significant development, we now show that it is possible to extract and detect both electrons and ions in coincidence onto a *single* detector by time switching the lens voltages appropriately. We have used one half of the existing coincidence apparatus, i.e., the electron detector of the two-detector setup, and have successfully measured electrons and ions in coincidence using a single velocity map imaging spectrometer with total flight length of 11 cm. Because we have used the electron detector of the two-detector coincidence setup as the detector for the single coincidence setup, the electron resolution is unaltered and will not be discussed here. The details are described in Ref. 11. The performance of the new one-detector coincidence setup is described in terms of ion mass resolution and coincidence data using femtosecond ionization data of Xe and CF_3I at 400 nm, respectively.

The present paper is organized as follows. In Sec. II, we present the apparatus. In Sec. III, we report the experimental data and we compare with data obtained using the standard two-detector coincidence imaging setup. We summarize our conclusions in Sec. IV.

II. EXPERIMENTAL

A. Vacuum and molecular beam

The coincidence imaging apparatus has been described in detail before and will be discussed only briefly here.[11,16,17] It consists of three differentially pumped UHV chambers, the source chamber, a buffer chamber and the imaging chamber. Improving upon the first series of experiments, which were done using a continuous molecular beam source,[11] in the present setup we use a home-built high-repetition rate (up to 5 kHz) cantilever piezo valve producing a pulsed molecular beam.[18,19] A pulsed molecular beam source matches well the duty cycle of the experiment because of the pulsed femtosecond laser source which operates at a repetition rate that is selectable between 1–5 kHz. The pulsed cantilever valve makes it possible to produce stronger beams and to use higher backing pressures. The piezo valve can operate both in pulsed mode and continuous mode and the gas was expanded through a nozzle with a diameter of 200 μm. In the present experiments, we operate the laser and the pulsed piezo valve at 1 kHz. Low seeding ratios of about 1% of CF_3I in neon and 5% Xe in neon are used, so as to avoid clusters in the molecular beam. The typical speed ratio with 3 bars backing pressure is about S = 25–30.[16]

a)Author to whom correspondence should be addressed. E-mail: m.h.m.janssen@vu.nl.

B. Laser system

The regen femtosecond laser (Spectra Physics Spitfire Pro) operates at 1 kHz and central wavelength of 800 nm. For multi-photon excitation of Xenon and CF_3I frequency doubled light of 400 nm with an energy of 15–20 μJ and a duration of about 170 fs is used. A half-wave plate is used to keep the polarization parallel to the plane of the imaging detectors. The laser beam is focused in the coincidence apparatus and crosses the molecular beam with a spot size of approximately 100 μm.

C. Single detector coincidence setup

In our new single detector coincidence setup presented here, we use only one position and time sensitive particle delay line detector (Roentdek large anode DLD40X[20]) for both electron and ion coincidence detection, see Fig. 1(a). The total ToF length is optimized for electron imaging, and equals 11 cm from the interaction region to the detector with a field-free ToF region of 5.25 cm. The charged particle lenses are used in pulsed mode to extract the electrons and ions toward the detector. The schematic of the operation is shown in Fig. 1(b). The repeller (R), extractor (E), and extra lens (L) are first set with appropriate negative voltages for electron velocity map imaging, i.e., R = −525 V, E = −385 V, and L = −270 V. Subsequently, about 200 ns after the laser interaction the voltages on all three lenses are quickly switched to a geometry for ion extraction, i.e., R = 2000 V, E = 1320 V, and L = 550 V. The positive voltages for ion extraction are retained for about 20 μs, sufficiently long for all ions to reach the detector. Subsequently, the voltages are switched back again in about 10 μs to electron extraction mode, so that when the next laser pulse arrives (1 ms inter pulse duration) the setup is ready for detection of electrons. All voltages are switched at the repetition rate of the laser system (1 kHz).

The HV switching causes ringing on the delay line and may lead to false events in the data. However, these false events due to switching are easily detected and rejected in the recorded TDC (time-to-digital converter) events of ions, as its time of occurrence (i.e., between 0.2 and 1.5 μs) is after the electron hit and before the arrival of most ions. The electrons are detected within 200 ns while the fastest ions arrive typically after about 1.5 μs under the imaging conditions. Therefore, all events recorded in between are rejected during data processing. Thus, the pick-up due to switching does not interfere with our correlated (e,ion) events. A typical TDC signal accumulated for 100 laser shots is shown in the bottom panel of Fig. 1(c). The electron, ringing, and ion signals are indicated.

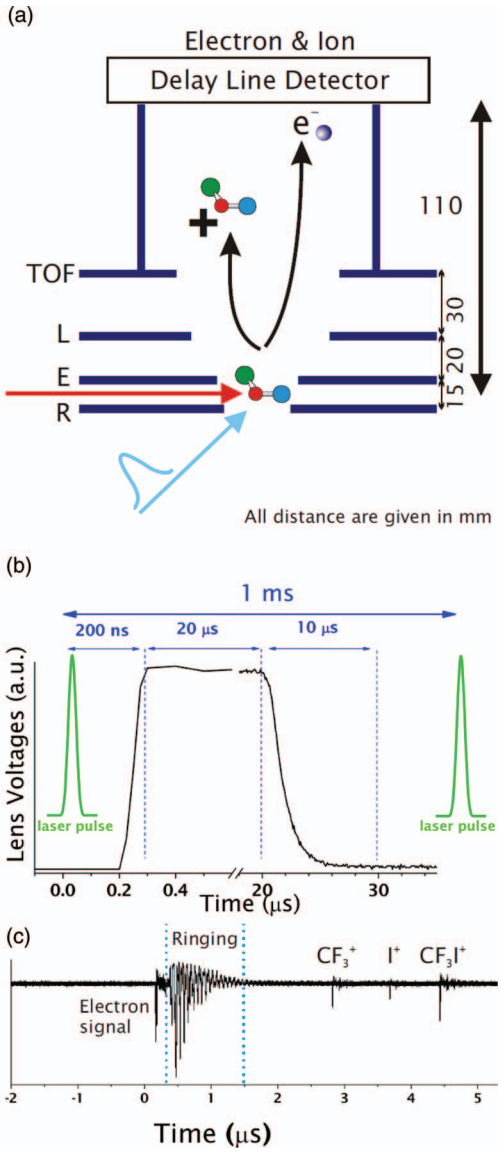

FIG. 1. (a) Schematic overview of the charged particle lenses and ToF tube for photoelectron-photoion velocity map coincidence imaging on a single detector. A pulsed molecular beam (red arrow), produced by a cantilever piezo valve,[18,19] is intersected by the laser pulses in the interaction region between charged particle lenses. Photoelectrons and photoions are extracted by switching the voltages on the charged particle lenses. (b) Schematic of the voltage conditions of a charged particle lens for electron and ion extraction. Before the laser interaction, the voltages are set to electron extraction mode and electrons are detected in the first 200 ns after the laser interaction. Thereafter, the voltages are switched in about 50–70 ns (Behlke HV switches) to detect ionic fragments. After 20 μs, sufficiently long after all masses of interest have reached the detector, the voltages are switched back in about 10 μs to the values for electron detection. All switching is at the repetition rate of the laser system (1 kHz in the present experiment). (c) The accumulated signal over 100 ms (100 laser shots) of the delay line detector as seen on an oscilloscope. The arrival of the electron, the ringing due to the high voltage switching and the arrival of various ions are clearly visible.

III. RESULTS AND DISCUSSION

A. Ion mass resolution

To characterize the ion mass resolution we have recorded the ion ToF spectrum obtained from multiphoton excitation of Xe with the frequency doubled laser output centered at 400 nm, see Fig. 2. The strongest five isotopes are clearly resolvable, the two weakest isotopes (^{128}Xe and ^{130}Xe) are discernible. The total ToF time is 3.8 μs with a FWHM Δt = 2 ns (for the strongest five isotopes). This corresponds to a mass resolution $\Delta m_{FWHM}/m \approx 1/950$.

The shorter length of the ToF tube in the case of the single detector setup essentially reduces the arrival time resolution and thereby the achievable mass resolution of the

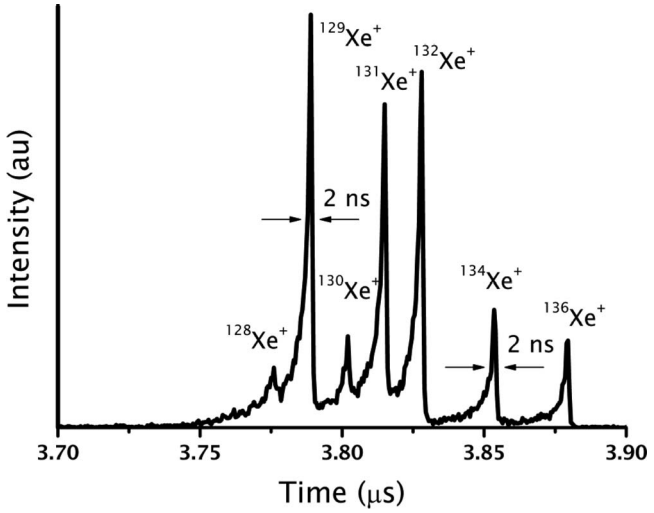

FIG. 2. Time-of-flight (ToF) spectrum of Xenon isotopes recorded from multiphoton excitation with femtosecond laser pulses centered at 400 nm in coincidence using our novel single detector coincidence setup. The ToF peaks have a FWHM $\Delta t = 2$ ns and a total ToF of 3.8 μs, which leads to $\Delta m_{FWHM}/m \approx 1/950$.

ions. This can be compared to the ion ToF-spectrum acquired using the two detector setup as reported before.[11] In the two detector case, the ion ToF tube had a length of 29.5 cm and the ions experience a total flight length of 35.2 cm from the interaction region to the detector. The reported ToF for the Xe isotopes was 8.3 μs with a FWHM $\Delta t = 2$ ns. This corresponds to a mass resolution $\Delta m_{FWHM}/m \approx 1/2000$ for masses near 130 amu. The shorter length of the flight tube in our new single detector coincidence setup reduces the ion mass resolution by a factor of two ($\Delta m_{FWHM}/m \approx 1/950$) while retaining the spatial resolution. However, for experiments with masses of $m \geq 14$, the mass resolution is still adequate enough to discriminate isotopes and mass peaks with $\Delta m \geq 2$ will be totally separated. One of the problems of the shorter ToF tube in the present single detector setup is detection of ion masses $m \leq 14$, as they coincide with the switching pickup on the detector. The ringing time cannot be easily reduced, and therefore the extraction field would have to be reduced for low masses. For a longer ToF tube, the ringing is never a problem since the first ions will arrive long after the ringing. The short length ToF was optimized for electron detection as part of the two-detector coincidence setup. It is certainly possible to design a better version with slightly longer tube clearly separating electrons, ions of all masses, and the intermediate pickup in time. Also, the short ToF length is not ideal for high-resolution three-dimensional slice imaging detection of ions.[21] Cases where the ionic fragment have low kinetic energy (or without any resolvable structure) are seen to have roughly the same spatial resolution (spread) irrespectively of the ToF length.

B. Single detector coincidence measurements

Coincidence measurements on CF_3I following single color (400 nm) multiphoton excitation have been previous reported using the two-detector coincidence setup.[22] To demonstrate that our novel single detector coincidence setup can be

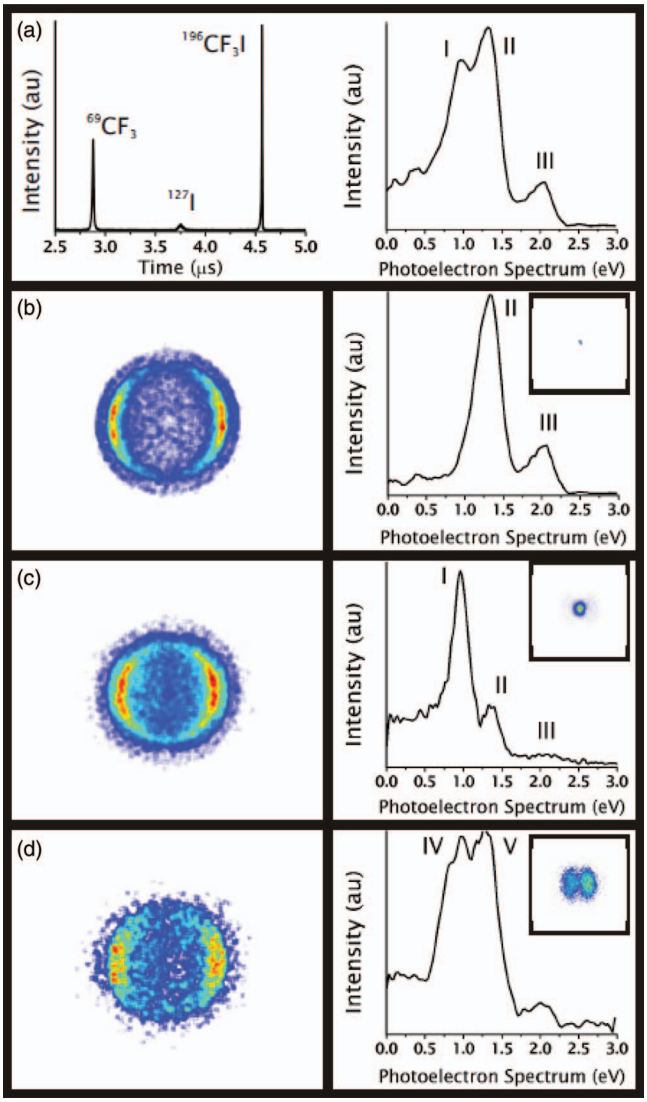

FIG. 3. Coincidence measurements on CF_3I obtained from multiphoton excitation with femtosecond laser pulses centered at 400 nm using the single detector setup. (a) Ion ToF spectrum (left) and photoelectron spectrum (right) of all events measured in coincidence. (b) Time sliced electron image, photoelectron spectrum, and ion image (insert) measured in coincidence with CF_3I^+ ions. (c) Time sliced electron image, photoelectron spectrum, and ion image (insert) measured in coincidence with CF_3^+ ions. (d) Time sliced electron image, photoelectron spectrum, and ion image (insert) measured in coincidence with iodine ions. The photoelectron kinetic energy values are listed in Table I. The ion images are shown for the same detector area.

used to study reaction dynamics without the loss of information, we have repeated the previous measurement using only the single detector setup. The results are depicted in Fig. 3. Panel (a) shows the total ion ToF spectrum (left) and the photoelectron spectrum (right) measured in coincidence with all these ions. The multiphoton excitation yields predominantly CF_3^+ (48.5%) and CF_3I^+ (44%), and a small amount of I^+ (7.5%). The appearance/ionization energy of the ions with the excess energy after four-photon excitation at 400 nm is listed in Table I. The photoelectron spectrum corresponding to all ions (CF_3^+, I^+ and CF_3I^+ together) shows predominately 3 peaks, labeled I, II, and III, around 1.0 eV, 1.3 eV, and 2.0 eV.

The photoelectron-photoion coincidence events of CF_3I^+, CF_3^+, and I^+ are shown separately in panel (b), (c),

TABLE I. Appearance energy/ionization potential for the production of the different ions after multiphoton ionization of CF_3I at 400 nm. The excess energy is given with respect to four-photon ionization (4 x hν = 12.4 eV), excess energy = 12.4 − AE/IP.

	AE/IP (eV)	Excess energy (eV)
CF_3^+, e^-	11.384 (Ref. 23)	1.03
I^+, e^-	12.78 (Ref. 24)	
CF_3I^+ ($X^2E_{3/2}$), e^-	10.37 (Ref. 25)	1.31
CF_3I^+ ($X^2E_{1/2}$), e^-	11.10 (Ref. 26)	2.04

and (d), respectively. The electron image is shown on the left-hand side and the corresponding photoelectron spectrum on the right-hand side. The insert pictures show the ion image. The size of the detector area is the same for all 3 cases in order to give a good indication of the ion kinetic energy.

The photoelectron image of CF_3I^+, panel (b), depicts two peaks with maxima at 1.32 eV (II) and 2.04 eV (III). These peaks can be assigned to the two ground states of CF_3I, the spin-orbit ground state $X^2E_{3/2}$, and spin-orbit excited state $X^2E_{1/2}$.

The channel leading to CF_3^+ and I is displayed in panel (c). The most dominant photoelectron peak is centered at 0.96 eV (I) and corresponds well to the excess energy of CF_3^+. Almost all of the excess energy is taken away by the electron and as a consequence the ion has very little kinetic energy. Two weaker peaks (II and III) are also discernible with maxima at 1.36 and 2.04 eV. The maxima and ratio of these peaks are identical to photoelectrons measured in coincidence with CF_3I^+ (panel (b)). All peaks (I–III) have also been observed using two-detector setup, see Fig. 2(c) in Ref. 22. The photoelectrons can be assigned to (in total) five-photon process. First a photoelectron is promptly ejected after absorption of four photons and the produced parent ion absorbs an additional photon and dissociates into CF_3^+.

The photoelectron-photoion coincidence events of I^+ are shown in panel (d) of Fig. 3. The appearance energy of this process lies above 12.4 eV, consequently this process is due to 5-photon excitation. The signal contribution from this channel is thus far weaker than the four-photon excitation needed to generate CF_3^+ and CF_3I^+, see panel (a). For this channel the excess energy is equal to (15.5–12.78 =) 2.72 eV. This energy can be distributed over the electron, the ion, and the neutral fragment. The dominant feature in the photoelectron spectrum is a broad peak between 1–2 eV, which has 2 centers located at 1.0 and 1.3 eV. The ion fragment has substantial kinetic energy, see insert. These two electron peaks have also been observed in the two-detector experiment. There the two peaks have been attributed to electrons ejected leaving the neutral parent just above the dissociation limit of $CF_3^+ + I$, but below the formation channel of $I^+ + CF_3$. Absorption of a fifth photon (before the dissociation is complete) opens the $I^+ + CF_3$ channel, resulting in ion fragments with substantial translational energy and internal excitation.

IV. CONCLUSIONS

We report a novel photoelectron-photoion coincidence imaging setup employing a single ToF delay line detector. By fast switching of the high voltages on ion optics we demonstrate that it is possible to obtain the complete three-dimensional momentum distribution of electrons and ions in coincidence using only a single detector. This new approach would reduce the building costs of a new coincidence imaging setup significantly while not compromising much on the experimental sensitivity and mass resolution.

ACKNOWLEDGMENTS

This research has been financially supported by the Council for Chemical Sciences of the Dutch Organization for Scientific Research (NWO–CW). The authors also acknowledge support by the European Union through the Integrated Infrastructure Initiative LaserLabEurope and the Marie-Curie Initial Training Network ICONIC. The authors gratefully acknowledge the excellent technical support by Mr. R. Kortekaas.

[1] M. Richard-Viard, O. Atabek, O. Dutiot, and P. M. Guyon, J. Chem. Phys. **93**, 8881 (1990).
[2] J. A. Davies, J. E. LeClaire, R. E. Continetti, and C. C. Hayden, J. Chem. Phys. **111**, 1 (1999).
[3] G. K. Jarvis, K. M. Weitzel, M. Malow, T. Baer, Y. Song, and C. Y. Ng, Rev. Sci. Instrum. **70**, 3892 (1999).
[4] P. Downie and I. Powis, Faraday Discuss. **115**, 103 (2000).
[5] M. Takahashi, J. P. Cave, and J. H. D. Eland, Rev. Sci. Instrum. **71**, 1337 (2000).
[6] R. E. Continetti, Annu. Rev. Phys. Chem. **52**, 165 (2001).
[7] M. Lebech, J. C. Houver, and D. Dowek, Rev. Sci. Instrum. **73**, 1866 (2002).
[8] J. Ullrich, R. Moshammer, A. Dorn, R. Dorner, L. P. H. Schmidt, and H. Schmidt-Bocking, Rep. Prog. Phys. **66**, 1463 (2003).
[9] A. M. Rijs, M. H. M. Janssen, E. T. H. Chrysostom, and C. C. Hayden, Phys. Rev. Lett. **92**, 123002 (2004).
[10] R. E. Continetti and C. C. Hayden, "Coincidence imaging techniques," in *Modern Trends in Reaction Dynamics*, edited by X. Yang and K. Liu (World Scientific, Singapore, 2004), pp. 475–528.
[11] A. Vredenborg, W. G. Roeterdink, and M. H. M. Janssen, Rev. Sci. Instrum. **79**, 063108 (2008).
[12] G. A. Garcia, H. Soldi-Lose, and L. Nahon, Rev. Sci. Instrum. **80**, 023102 (2009).
[13] X. Tang, X. Zhou, M. Niu, S. Liu, J. Sun, X. Shan, F. Liu, and L. Sheng, Rev. Sci. Instrum. **80**, 113101 (2009).
[14] A. T. J. B. Eppink and D. H. Parker, Rev. Sci. Instrum. **68**, 3477 (1997).
[15] *Imaging in Molecular Dynamics, Technology and Applications*, edited by B. J. Whitaker (Cambridge University Press, Cambridge, 2003).
[16] A. Vredenborg, C. S. Lehmann, D. Irimia, W. G. Roeterdink, and M. H. M. Janssen, ChemPhysChem **12**, 1459 (2011).
[17] C. S. Lehmann, N. B. Ram, D. Irimia, and M. H. M. Janssen, Faraday Discuss. **153**, 173 (2011).
[18] D. Irimia, R. Kortekaas, and M. H. M. Janssen, Phys. Chem. Chem. Phys. **11**, 3958 (2009).
[19] D. Irimia, D. Dobrikov, R. Kortekaas, H. Voet, D. A. van den Ende, W. A. Groen, and M. H. M. Janssen, Rev. Sci. Instrum. **80**, 113303 (2009).
[20] See http://www.roentdek.com for MCP delay line detector manual, version 9.
[21] M. L. Lipciuc, J. B. Buijs, and M. H. M. Janssen, Phys. Chem. Chem. Phys. **8**, 219 (2006).
[22] A. Vredenborg, W. G. Roeterdink, C. A. de Lange, and M. H. M. Janssen, Chem. Phys. Lett. **478**, 20 (2009).
[23] R. L. Asher and B. Ruscic, J. Chem. Phys. **106**, 210 (1997).
[24] F. Aguirre and S. T. Pratt, J. Chem. Phys. **118**, 6318 (2003).
[25] N. A. MacLeod, S. Wang, J. Hennessy, T. Ridley, K. P. Lawley, and R. J. Donovan, J. Chem. Soc., Faraday Trans. **94**, 2689 (1998).
[26] L. D. Waits, R. J. Horwitz, R. G. Daniel, J. A. Guest, and J. R. Appling, J. Chem. Phys. **97**, 7263 (1992).